SAND2022-8498C

Sandia National Laboratories

# Fracture Detection of Lab Scale Energetic Stimulation

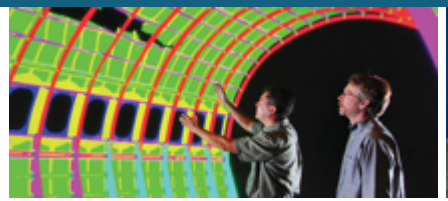

Sandia National Laboratories: Eric Robey, Joseph Pope

Lawrence Livermore National Laboratory: Oleg Vorobiev

New Mexico Institute of Mining and Technology:

Sivana Torres, Michael Hargather, Dillon Mann, Jamie Kimberley

ARMA Santa Fe: June 27, 2022

U.S. DEPARTMENT OF ENERGY | NNSA National Nuclear Security Administration

Sandia National Laboratories is a multimission laboratory managed and operated by National Technology & Engineering Solutions of Sandia, LLC, a wholly owned subsidiary of Honeywell International Inc., for the U.S. Department of Energy's National Nuclear Security Administration under contract DE-NA0003525.



Sandia National Laboratories is a multimission laboratory managed and operated by National Technology & Engineering Solutions of Sandia, LLC, a wholly owned subsidiary of Honeywell International Inc., for the U.S. Department of Energy's National Nuclear Security Administration under contract DE-NA0003525.

# Introduction

Goal: Create connectivity between wellbores within a geothermal the reservoir

Energetics based stimulation to

Position Orientation Timing (POTs)

- Scaled Experimentation
  - Engineer geologic artifacts (stresses, layers, flaws)
  - Study the effects of energetics on the artifacts relative to their position and orientation to artifacts
  - Understand ability of energetics to enhance EGS connectivity
- Simulation
  - Study the interactions available from scaled experimentation
  - Increase the model fidelity based on testing
  - Optimized position orientations and timing

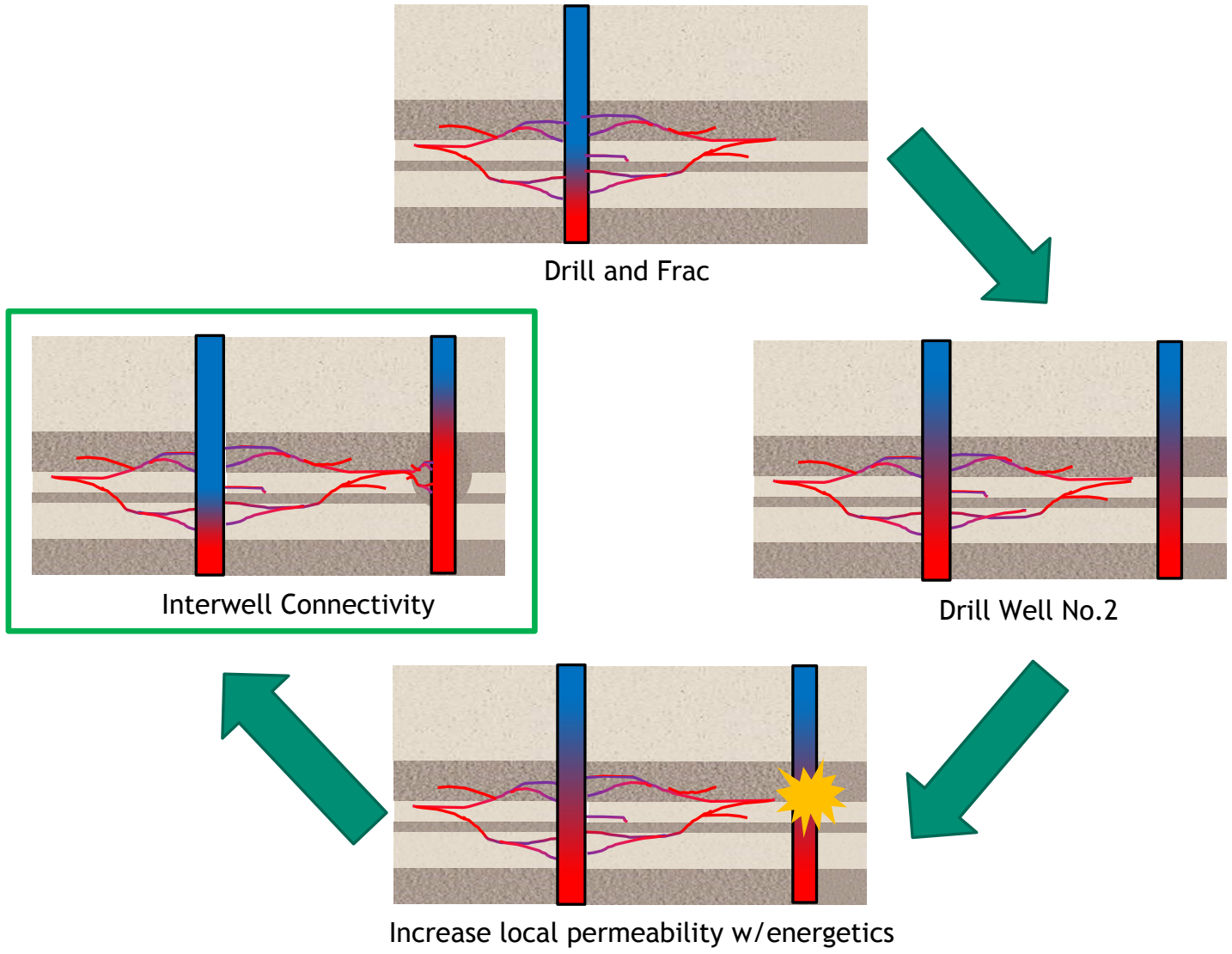

# Motivation for Energetics EGS

## Energetic Stimulation

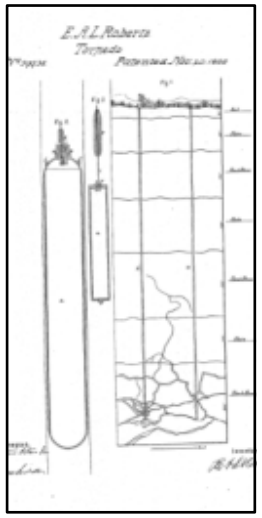

US Patent 59,936 (1866)
Roberts Torpedo Company

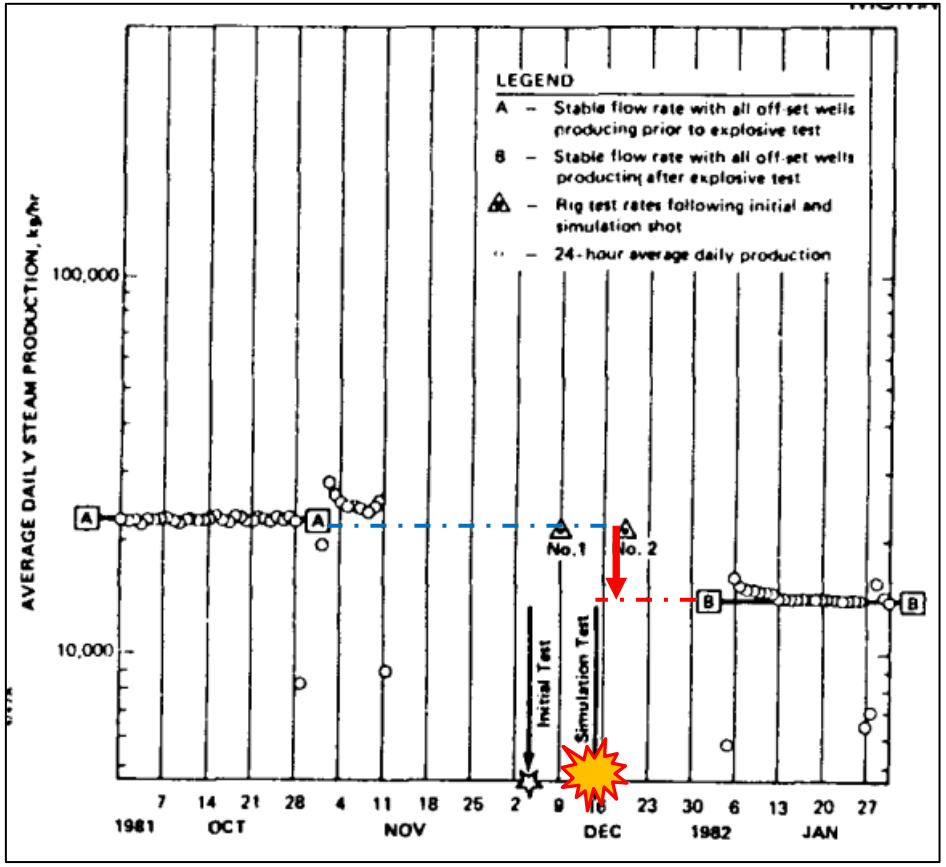


Reduced Production: LF-30 (Geysers Field, USA)
(Mumma et. al, OSTI 5093502, 1982)

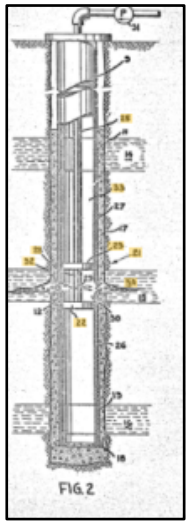


US Patent 2,642,142 (1953)
Stanolind Oil & Gas Company

## Hydraulic Stimulation

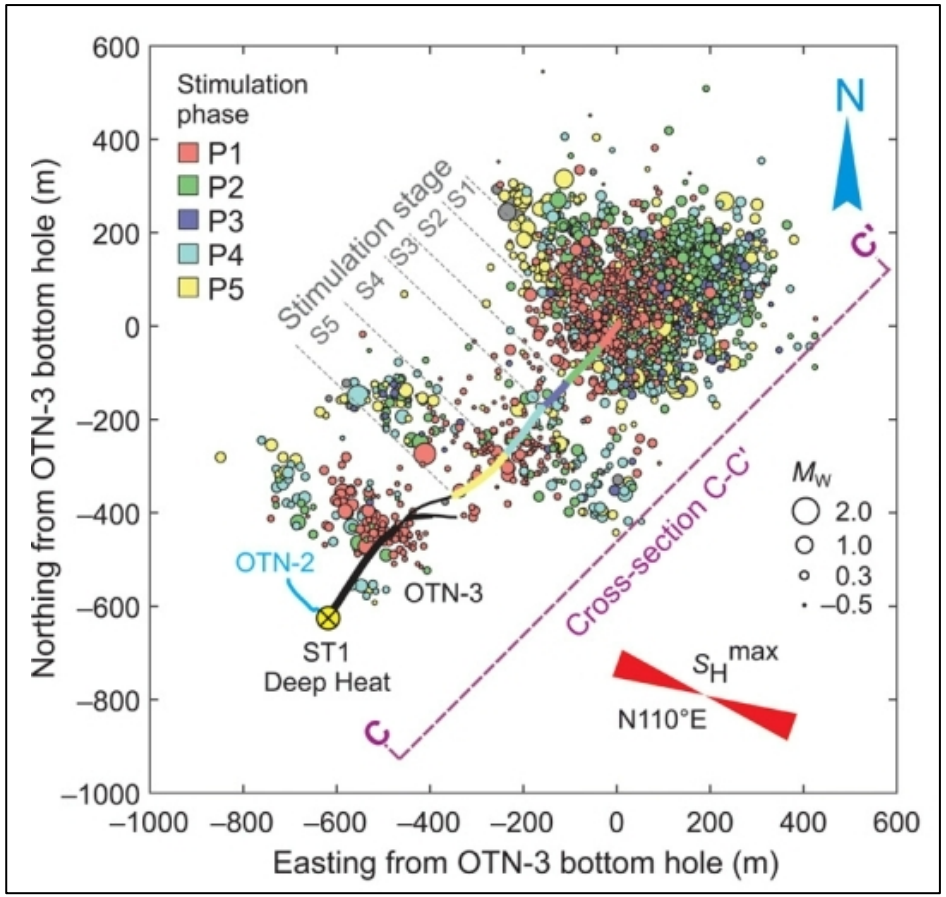


Induced Seismicity: OTN-3 Well (Helsinki, Finland)
(Kwiatek et. al, AAAS, CC BY-40, 2019)

# Scaling EGS physics to improve models

Field Scale
$10^2$-$10^3$ meters in scale
$10^6$ USD

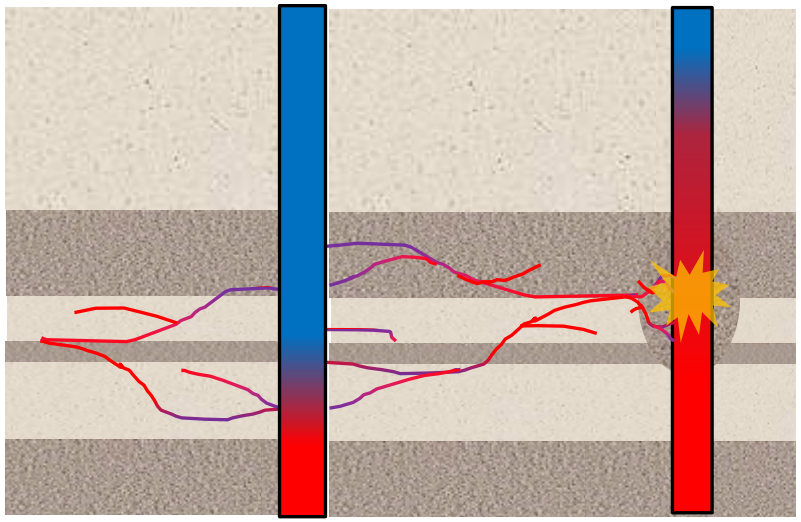

Lab Scale using Engineered & Natural materials
$10^{-1}$-$10^0$ scale
$10^2$ - $10^3$ USD

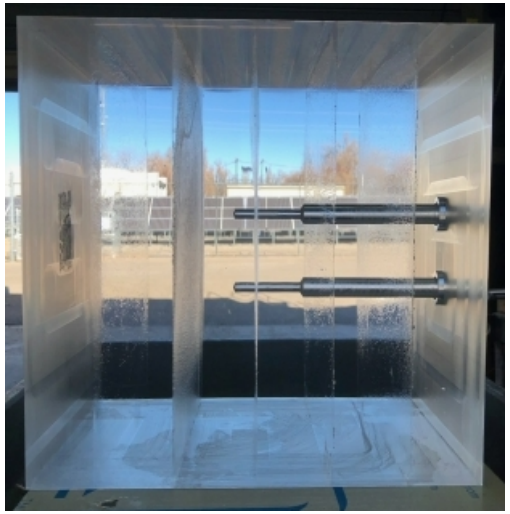

- Time, Cost, Uncertainty and Risk are reduced
- Experiments can be rapidly configured to study effects of stresses, flaws and emplacements
- Physics of subsurface can be directly observed using high speed diagnostics
- Computational models can evaluate a matrix of experimental configurations
- Computational models can be evaluated against experiments

# Computational Guidance

## Wellbore Isolation Effects in PMMA (~85 µs)

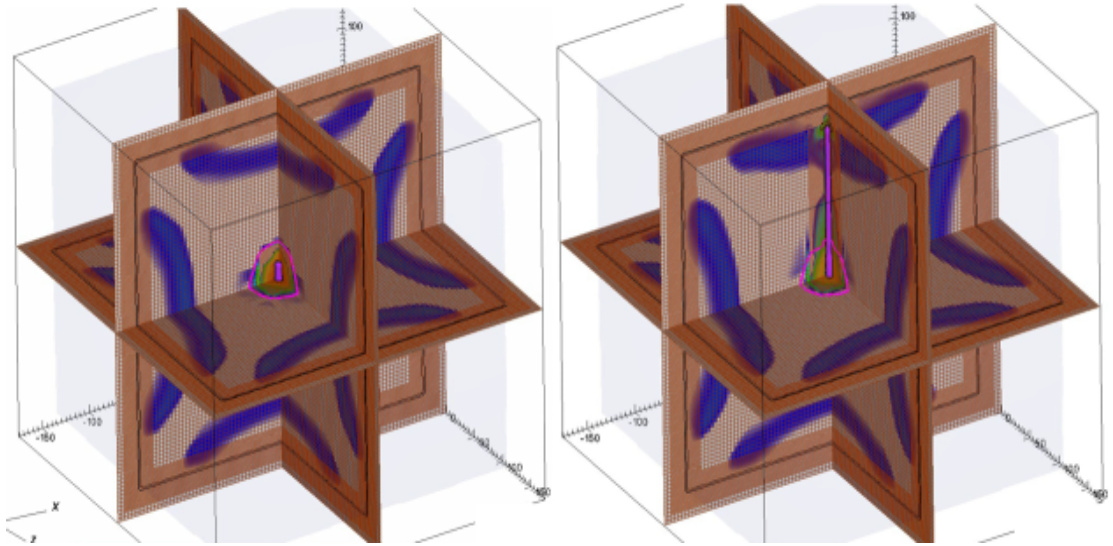

Isolated
(Above and Below Source)

Non-Isolated

## Wellbore Construction Effects in PMMA

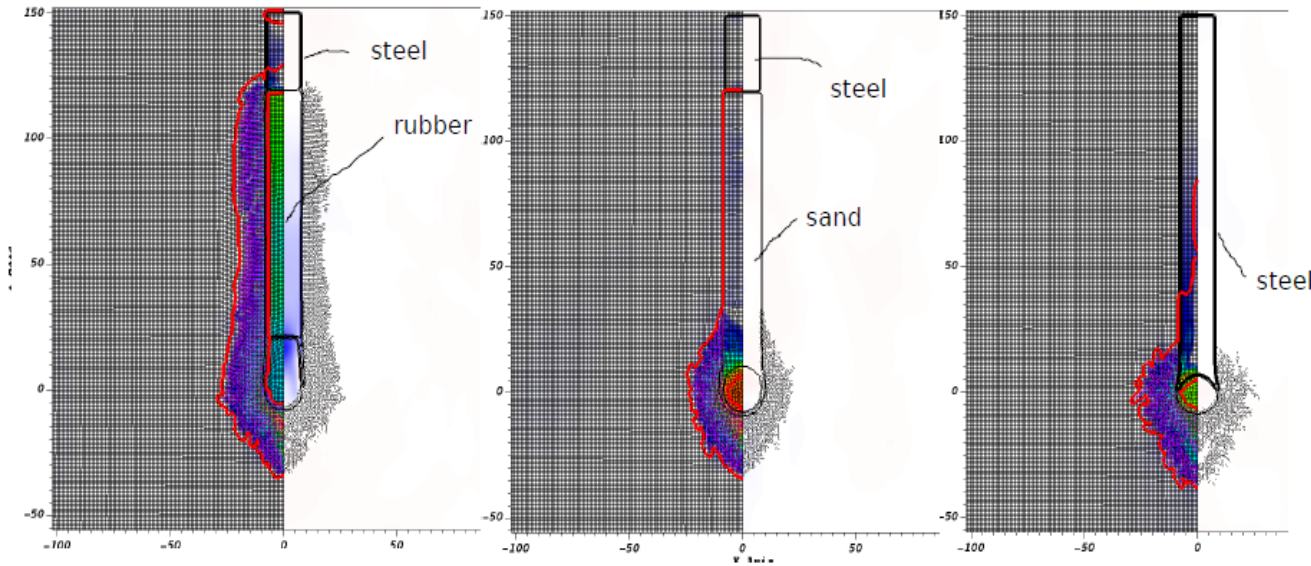


A

Open Hole filled w/rubber
Damage away from source

B

Open Hole filled w/sand
Damage local to source

C

Cased Hole just above source
Damage to casing

# Experimental Setup

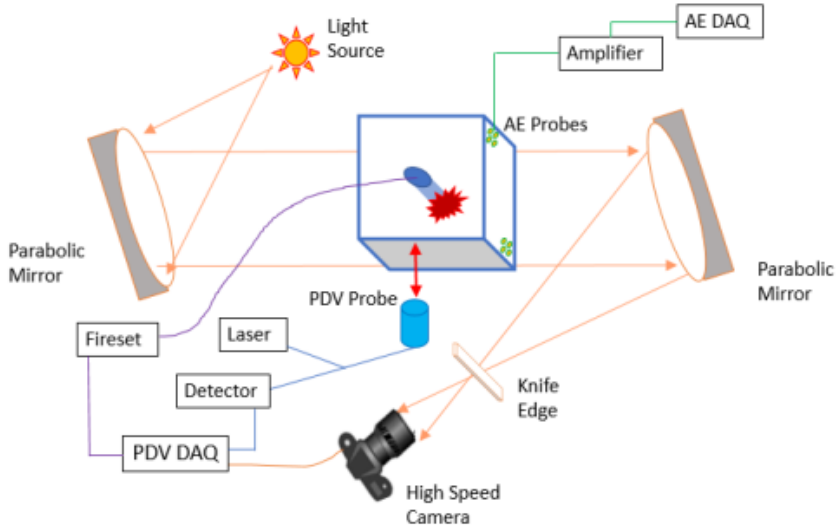


Shadowgraph Imaging
SHOCK & FRACTURE

- Capture density changes in the sample by observing the change in refractive index due to shock or fracture
- High speed cameras allows the tracking of features moving through the material by pixel evaluation

Photon Doppler Velocimetry (PDV)
SHOCK

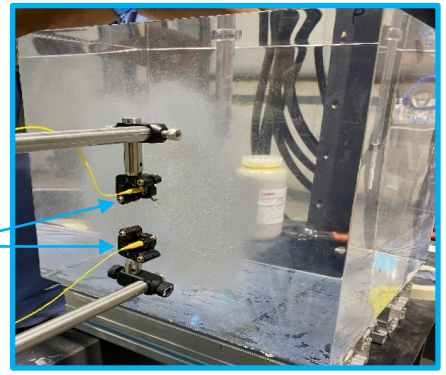


- Capture particle velocity on a samples surface due to strong waves (shock) via Fourier transform of laser interferometry
- Non contact probe measures difference of beat frequency difference upon movement of a surface

Acoustic Emissions(AE)
FRACTURE

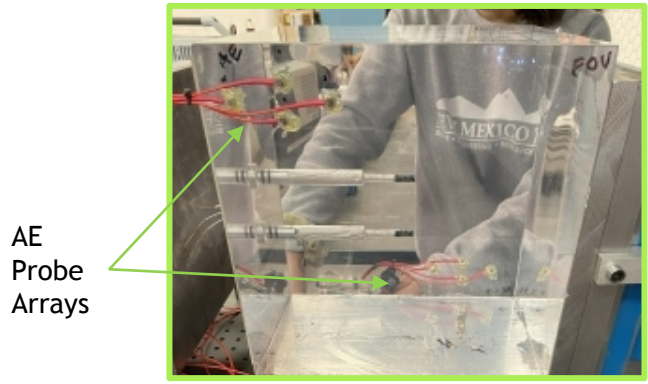


- Capture emitted waveforms from discrete spatial-temporal sources (fractures)
- Contact probe array measures waveforms to observe arrival for co-location of a source using multiple channels

# Shadowgraph Results (PETN Source)

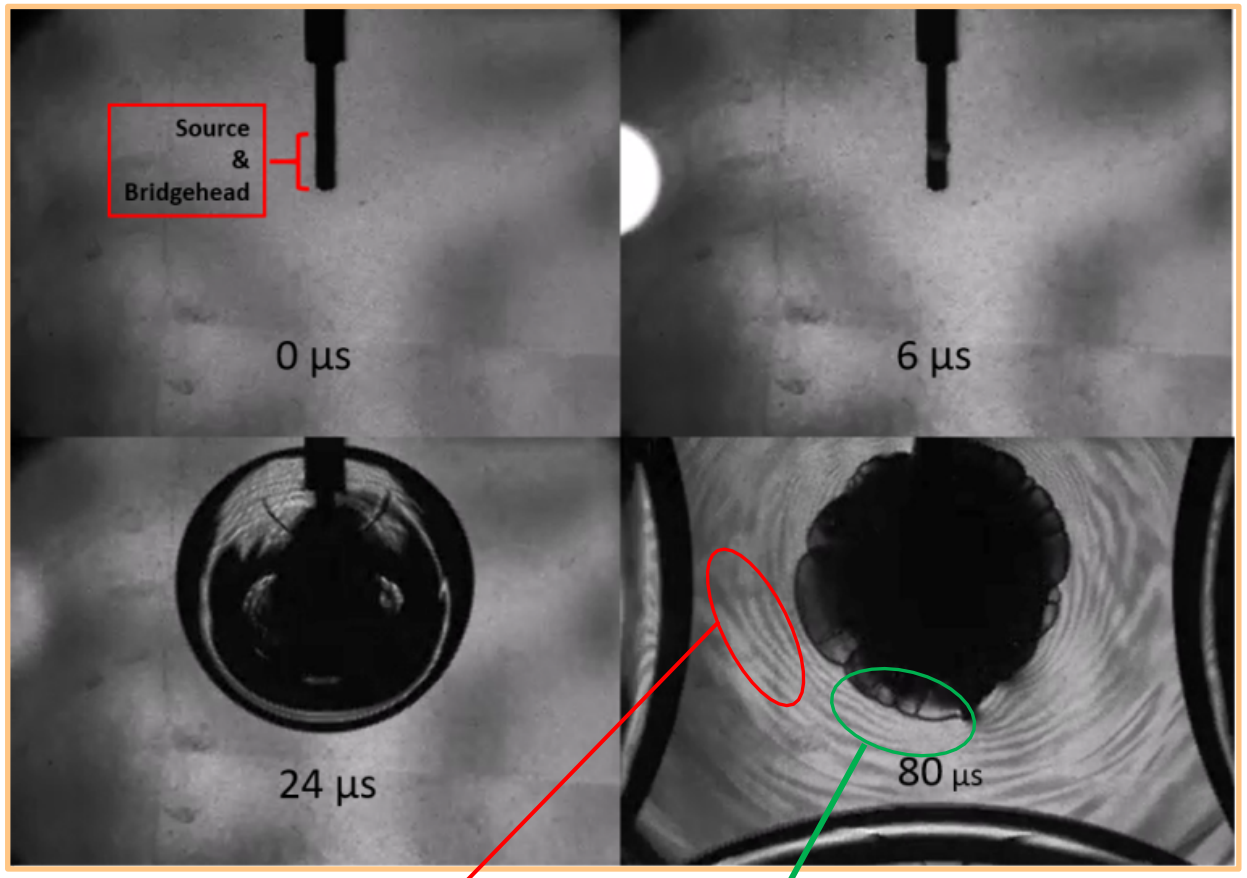


- 6 µs- First shock from source extending just into the near wellbore region
- 24 µs- Primary shock can be seen moving away from wellbore
- 40 µs (not shown)- coherent fractures begin to extend beyond darkened region
- 80 µs- reflections from primary shock observed re-enter field of view
- 80 µs alternating light gray and gray bands (stress waves) emanate from locations other than the source suggest secondary energy release near fracture tip
- Near source and adjacent volumes rendered opaque in later time due to a combination of increased number of fractures, orientations of, and filling with product gasses

# Shadowgraph to PDV correlation of shock (PETN Source)

Streak Image (Shadowgraph derived U)

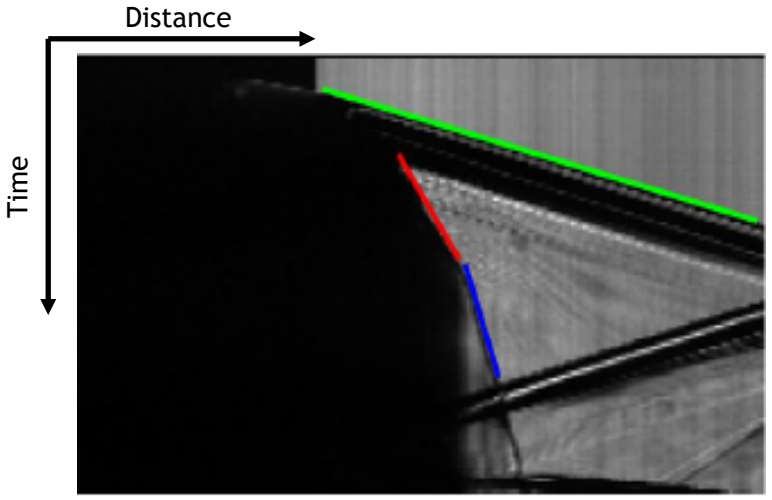


Free Surface Velocity (PDV)

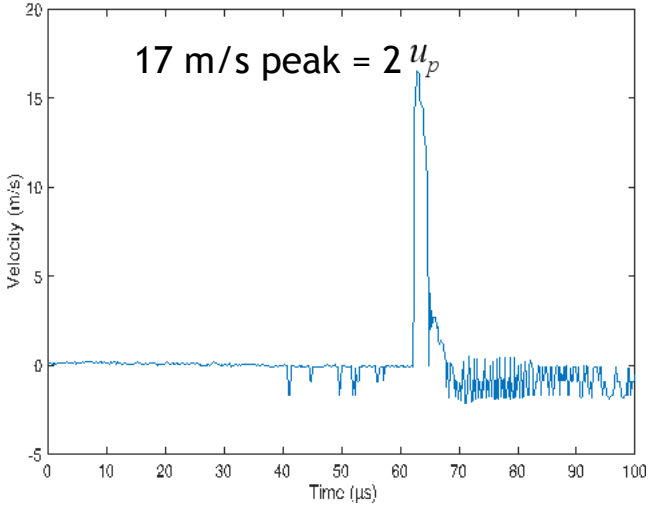


$$(1)\quad U_s = 6.486u_p^{\,3} - 7.823u_p^{\,2} + 3.549u_p + 2.703$$

Wave velocity based on curve fits: (Jordan et. al, J. Dyn. Behavior Mat, 2019)

| PDV Derived (km/s) | Shadowgraph Derived (km/s) | Difference (%) |
|---|---|---|
| 2.73 | 2.80 | 2.5 |

<u>Shadowgraph</u>

- Post processed shadowgraph streak images can be used track shock front (U)
- Slope of pixel column is inverse of wave velocity
  (less slope = greater velocity)
- Wave front in green moving faster than fracture fronts (red & blue)

<u>PDV</u>

- Jordan et. al generated curve fits for planar shocks velocities (U) as a function of internal surface particle velocities ($u_p$) per Eq (1).
- Free surface is being observed, collected value is really 2X of an internal surface for use in Eq (1).
- Shock in this case is also spherically growing so probe position on cube's surface can influence data
- ***PDV is great for shock, but what about fractures?***

# Acoustic Emissions Results (RP-80 Source)

AE Source Locations vs Time ($\sigma_y$ is 2 MPa)

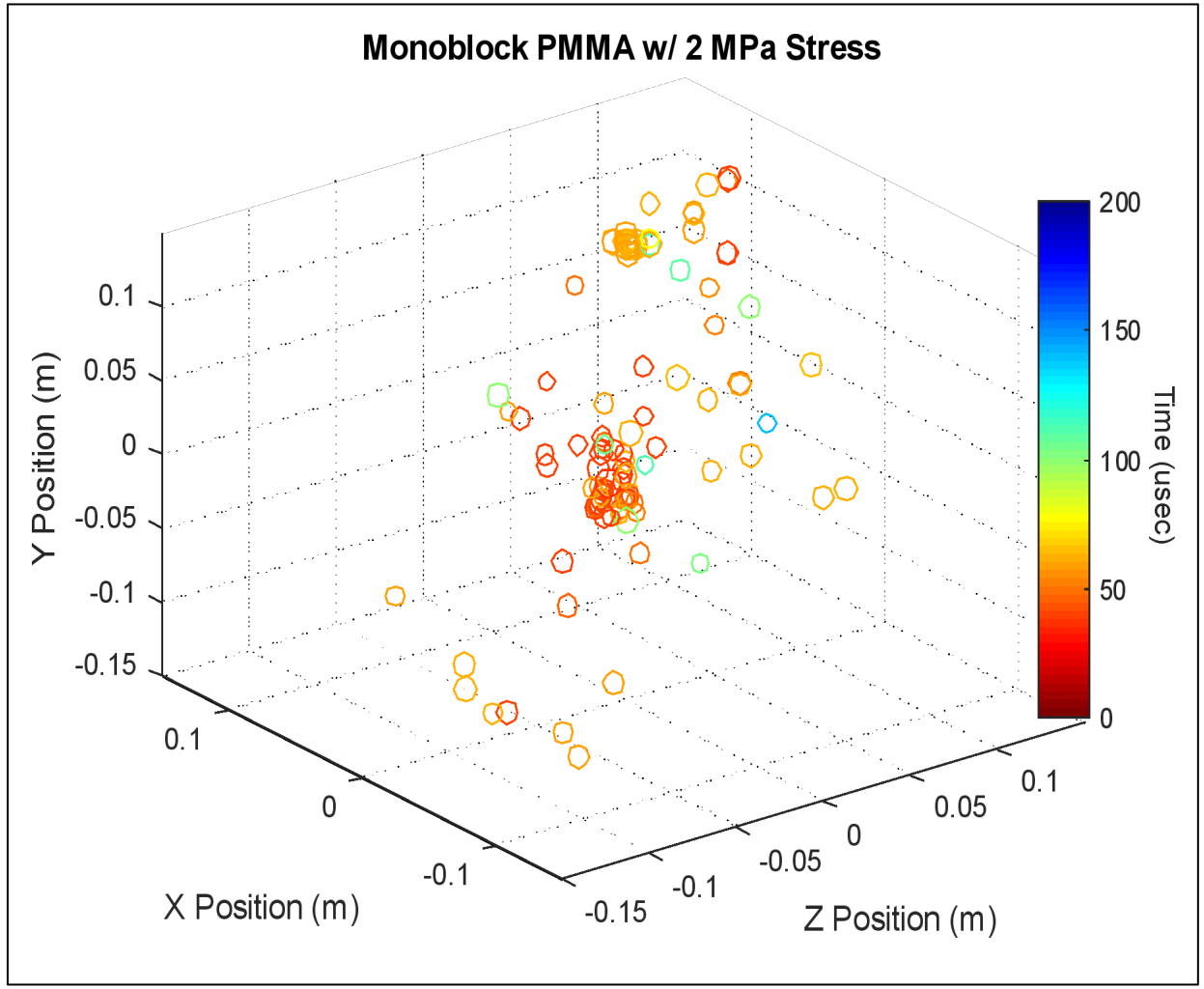


Acoustic Emissions

- Waveforms captured by 2 arrays (4 channels each)
- System sampled at 10 e6 samples/s (Msps)
- Between 50-200 emissions correlated per test
- Color indicates time, size indicates signature magnitude

AE vs Post Test Artifact

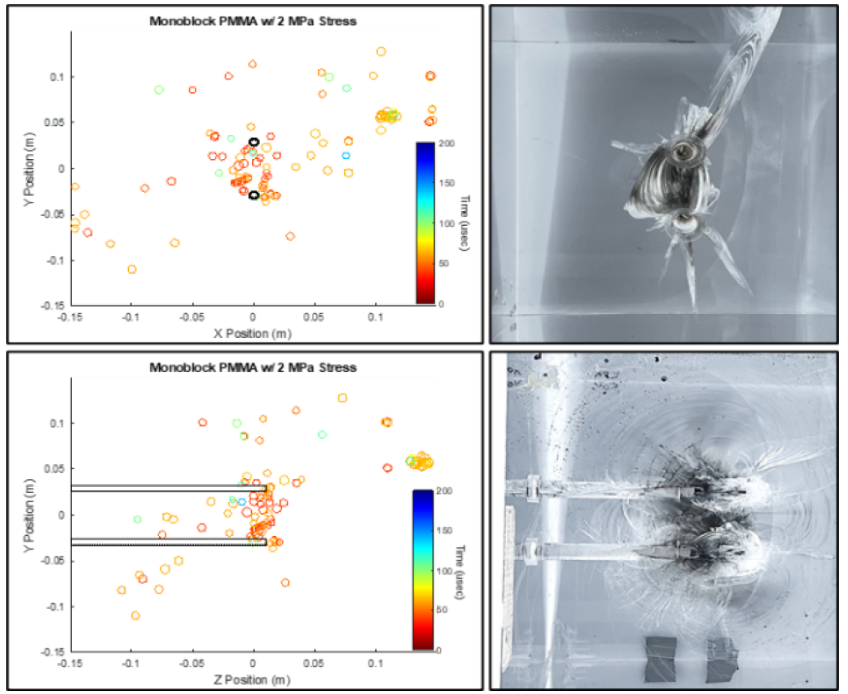

# Acoustic Emissions Correlation to Shadowgraph (RP-80 Source)

## AE Source Locations vs Time

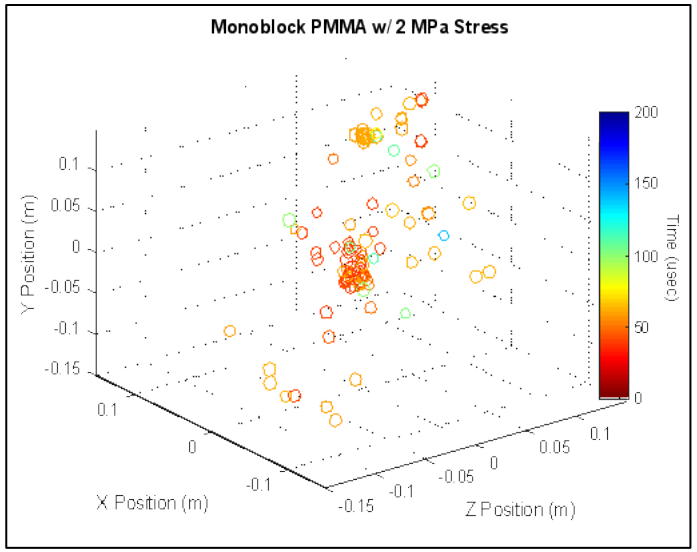


AE of stressed monoblock. $\sigma_1$ applied along the Y-axis. FOV along X. Darker colors correlate to later arrivals (µs). Marker size indicates relative emission amplitude.

## AE Locations vs Shadowgraph

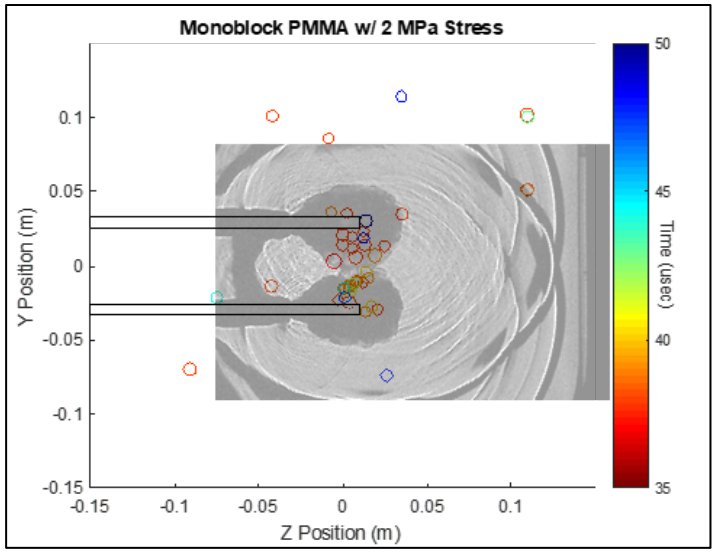


Scaled shadowgraph at 50µs overlaid on AE (0-50 µs) of stressed monoblock. Boreholes represented by black rectangles.

(1) $$\gamma_i = \frac{\sqrt{(x_i - x_s)^2+(y_i - y_s)^2+(z_i - z_s)^2} - \sqrt{(x_1 - x_s)^2 + (y_1 - y_s)^2+(z_1 - z_s)^2}}{v}$$

(2) $$\square_{\square} = \square_{\square\square} - \square_{\square\square}$$

(3) $$\chi^2 = \Sigma(\gamma_i)^2$$

Nelder, J.A., and R. Mead. 1965. A Simplex Method for Function Minimization. The Computer Journal. 4: 308-313

Ge, M. 2003 Analysis of source location algorithms part II: iterative methods[J]. Journal of Acoustic Emission 21(1), 29–51

Mistras Group. 2014. Express-8 AE System User's Manual

## Acoustic Emissions (3D)

- Uniform media with constant wave speed v
- Three sensors may be used to derive an x, y, and z of source
- A 4th sensor can derive $\gamma$; a difference in waveform arrival for the array (calculated vs observed)
- "Guesses" for the x, y, z location of wave forms are made until the regression sum $\chi$ is minimized

## Shadowgraph(2D)

- Planar expansion of spherical sources are observed by the change in refractive index in the YZ plane
- Features in and out of plane may be substantially obscured or underestimated in speed
  - I.E. Feature with a substantial component in the X direction that cannot be discriminated

# Fracture Velocity Correlation (RP-80 Source & Layered Cube)

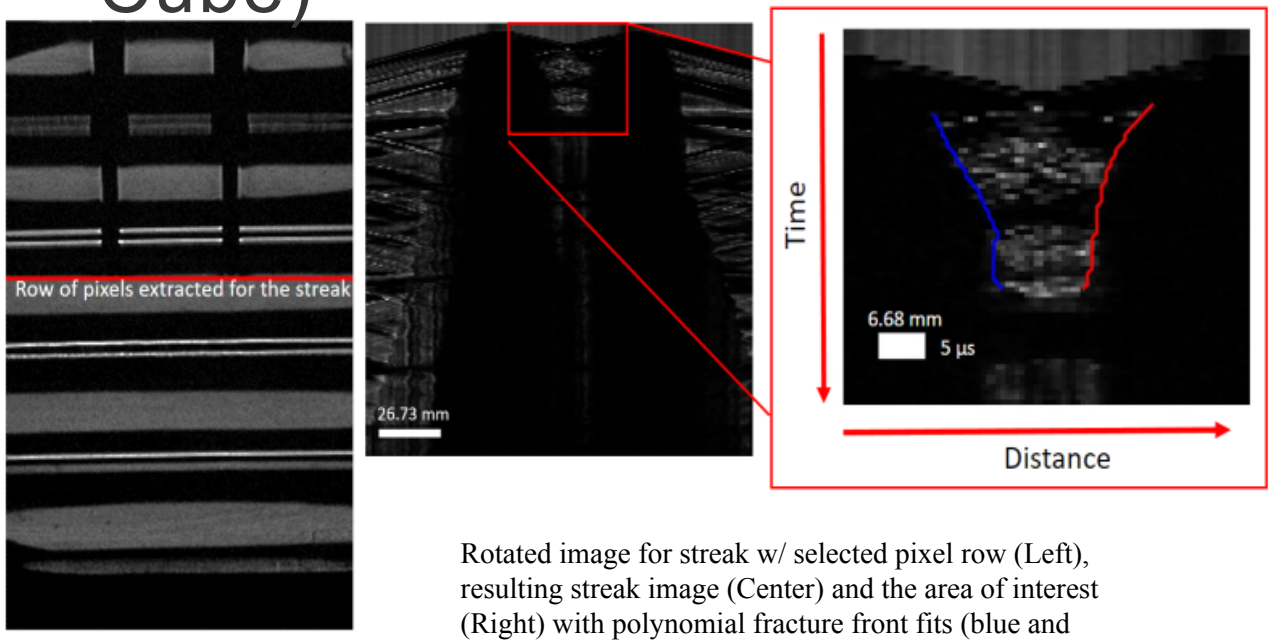


Rotated image for streak w/ selected pixel row (Left), resulting streak image (Center) and the area of interest (Right) with polynomial fracture front fits (blue and red).

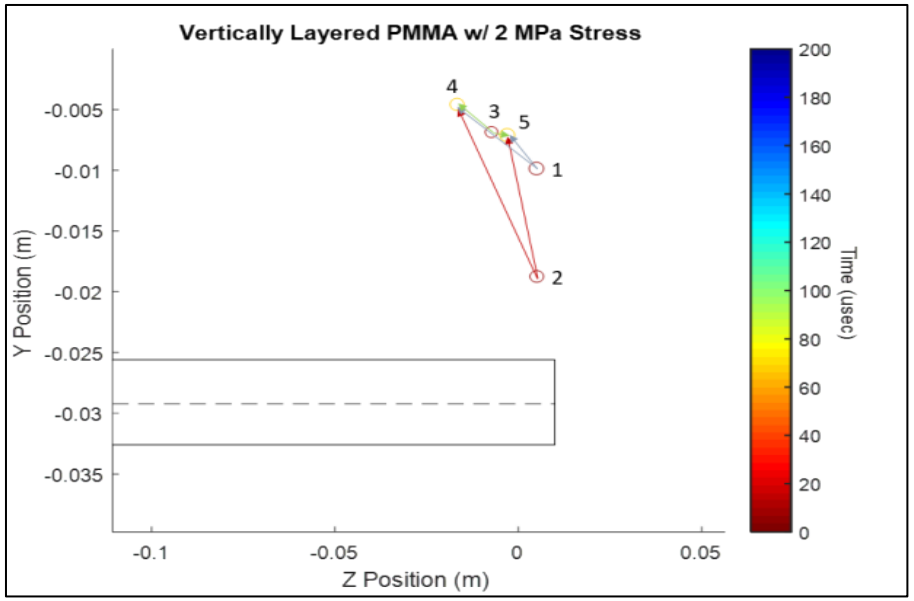


AE of layered and stressed cube in the ZY plane. Isolated by emission location and time w/ 6 possible fracture paths. Lower bore represented by rectangle, upper bore not shown. $\sigma_1$ applied along the Y-axis,

Post Processing Shadowgraph (2D)

- Extract a pixel row to create streak image to track the fracture front
- Right going fracture front (blue) @ 323 m/s
- Fit by polynomial, reasonable value compared to previous research (Kobayashi, 1974; 380 m/s) for Mode I growth in high strain rates with wire break detection method

Acoustic Emissions (3D)

- Interrogate data to look for fracture front location vs time (I.E. fracture velocity)
- Filter data by looking at a volume of interest near a prompt emission
- Calculate multiple $\sqrt{dx^2 + dy^2 + dz^2}/dt$
- Growth-Arrest-Growth may not accurately capture "velocity" over these distances & time scales

| | 3D & (2D) Velocity (m/s) | |
|---|---|---|
| Points | P4 | P5 |
| P1 | 387 (359) | 279 (136) |
| P2 | 584 (418) | 556 (228) |
| P3 | 363(166) | 435(74) |

*Expect observed velocities to be lower than Mode I observations (Kobayashi) due to stress cage effect of source*

# Discussion of Acoustic Emissions

## AE vs Post Test Artifact (Stressed)

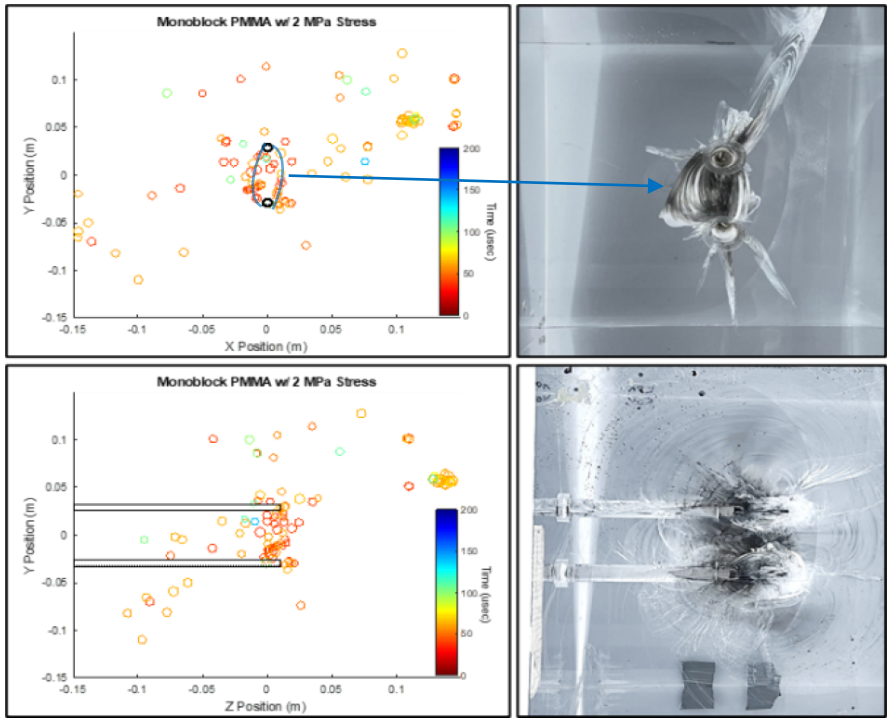


AE of stressed monoblock (Left) and Photo (right) in the XY (Top) and ZY (Bottom) planes. Boreholes represented by black circles or rectangles. $\sigma_1$ applied along the Y-axis

## AE vs Post Test Artifact (Layered & Stressed)

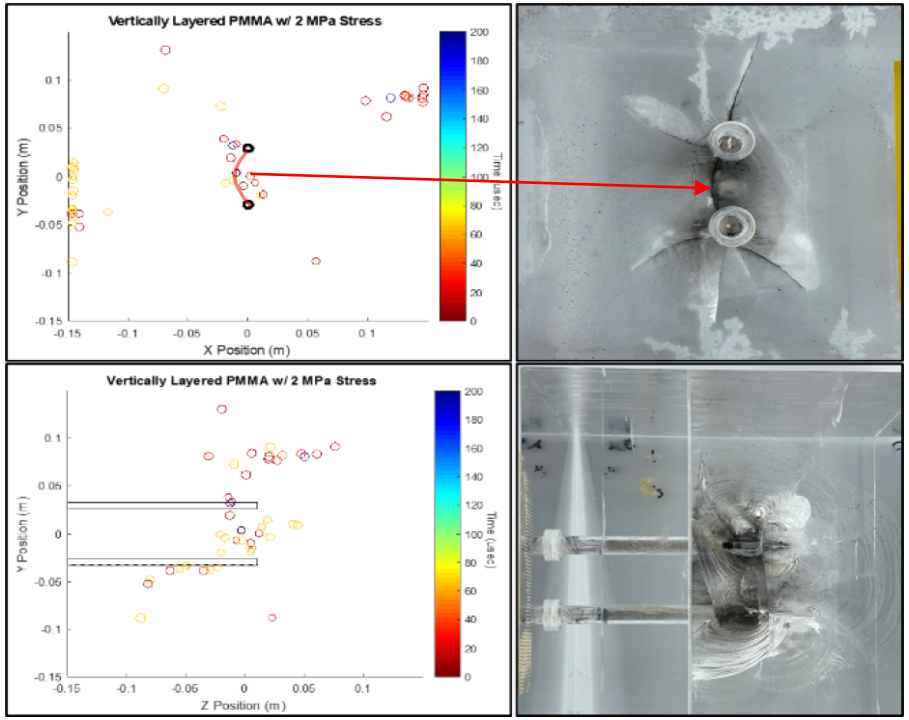


AE of layered and stressed cube (Left) and Photo (right) in the XY (Top) and ZY (Bottom) planes. Boreholes represented by black circles or rectangles. $\sigma_1$ applied along the Y-axis

Comments

- Early time fractures near the wellbores and in the inter-well volume appear to be captured
  - Elliptical network in Blue (left top) vs curved network in Red (right top)
- False/missed emissions are due to several factors
  - Emissions from source to sensor are attenuated through fracture, damage or delaminated materials (over 200 samples for intact vs 60 for delaminated blocks)
  - Differences in bulk material velocity means algorithm breaks down (regression criteria deteriorates as time/damage increase)
  - Strong waves persist in the volume due to primary shock and strong reflections
    - Hardware constraints such as recovery time for sensors cause data rejection
  - Studies of this scale are worst case…. Small volumes with fast source/reflected waves; a highly challenging temporal-spatial resolution problem

# Discussion

## Conclusions

- Shock is well correlated within 2.5% across PDV and shadowgraph diagnostics
- Stress state ***did*** change the preference for fracture orientation (0 vs 2 MPa) despite using a fast rise time source (may evolve Cuderman's understanding)
- Acoustic emission detection was added to capture 3D fracture network creation/growth in transparent materials
- Confidence has been gained by employing AE to the PMMA reservoirs with dual explosive sources, use of slower/lower shock sources expected to improve results in geologic materials
- Better placement & more AE sensors/arrays are better as they can be isolated from the "action" by a prompt fracture or delamination hiding emissions from a later time active source
- Laminated reservoirs or surrogate contact creates challenges/limitations to sensing weak waves
- This test series is the first known successful application of AE technology in the presence of explosives….especially in a small scale…. proof of concept it worked exceptionally well.

## Future work

- Geologic materials with AE sensing with fast (same as this phase) and slower sources
- Increased size geologic reservoirs (granite) with more sensors
- Develop cross correlation tools for AE data comparisons against geologic post mortem CT scans
- Improvements to capture & processing of acoustic emission data to inform computational model

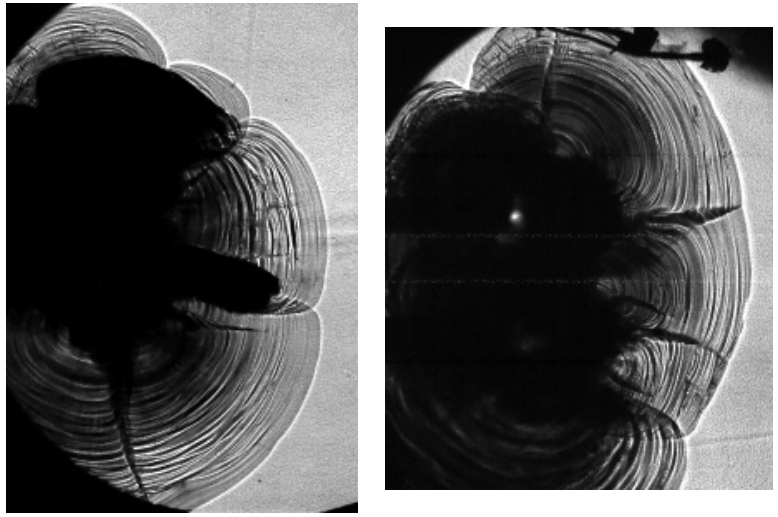

Monoblock fractures at 600 μs(unstressed left; stressed vertically right) w/ same Field of View

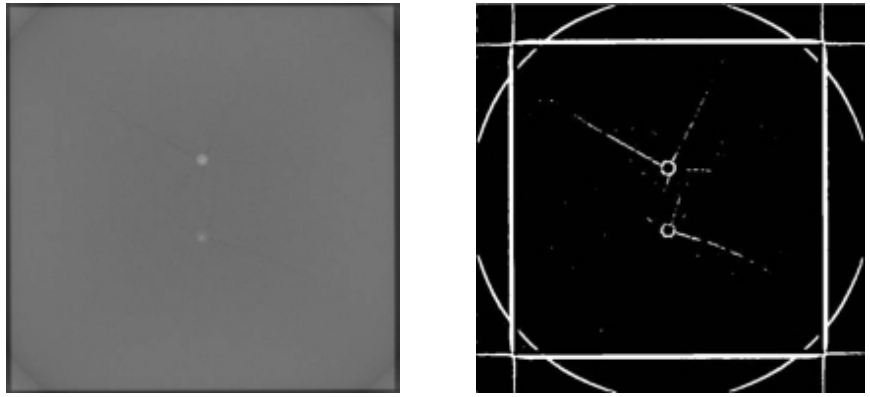

CT layer of stimulated cube (raw left; image processed right) w/1e-17 $m^2$ of unconnected fracture network

# Acknowledgements

Sandia National Laboratories is a multi-mission laboratory managed and operated by National Technology and Engineering Solutions of Sandia, LLC., a wholly owned subsidiary of Honeywell International, Inc., for the U.S. Department of Energy's National Nuclear Security Administration under contract DE-NA-0003525.

This work was sponsored by the Geothermal Technology Office of the U.S. Department of Energy.

The work by Lawrence Livermore National Laboratory was done under Contract DE-AC52-07NA27344

Funding for this work at New Mexico Institute of Mining and Technology (New Mexico Tech) is provided by Sandia National Laboratories via PO 2179527.

# References


1. EPA. 2016, Hydraulic Fracturing for Oil and Gas: Impacts from the Hydraulic Fracturing Water Cycle
2. Grubelich, M., 2015. An Overview of High Energy Stimulation Techniques for Geothermal Applications. *OSTI. 1248651, SAND2015-2614C*
3. Mumma, D., McCullough, F., Schmidt, E.W., Pye, D.S., Allen, C.W., Pyle, D., and R.J. Hanold. 2015. GEOFRAC- An Explosives Stimulation Technique for a Geothermal Well of High Energy. *Geothermal Resource Council Meeting, 11-14 October 1982. LA-UR-82-2020*
4. Cuderman, J.F., Chu, T.Y., Jung, R.D, and R.D. Jacobson. 1986. High Energy Gas Fracture Experiments in Fluid-Filled Boreholes- Potential Geothermal Application, Sandia National Laboratories, SAND85-2809
5. Robey, R.E., Pope, J.S., Vorobiev, O.Y., Torres, S.M., Hargather, M.J., Kimberley, J., Mann, D., 2021. Lab Scale Study of Energetic Gas Stimulation in Engineered Materials. 55th US Rock Mechanics/Geomechanics Symposium. ARMA 21-1219
6. Bastea S., Fried L.E., Glaesman K.R., Howard W.M., Kuo I.F., Nimmakala S., Souers P.C., Taller D., and P.A. Vitello. 2019. CHEETAH 9.0 User's Manual, Energetic Materials Center, Lawrence Livermore National Laboratory, LLNL-SM-769619
7. Rae P.J., A Review of the Mechanism by which EBW Detonators Function, Los Alamos National Laboratory, LA-UR-18-31181, 2018
8. Cooper, P.W. 1994. *Explosives Engineering*. 1st ed. Hoboken NJ: John Wiley and Sons.
9. Settles, G.S., 2001. *Schlieren and Shadowgraph Techniques: Visualizing Phenomena in Transparent Media.* Berlin: Springer.
10. Jordan J.L., Casem D., and Zellner M., 2019. Shock Response of Polymethylmethacrylate. J. Dynamic Behavior of Mater. 3: 372–78
11. Ward, S., Braithwaite, C., and A. Jardine. 2017. The Effects of Nanostructure upon the Dynamic Ductile Fracture of High Purity Copper, Procedia Engineering, DYMAT 23rd Technical Meeting-International Conference on Dynamic Fracture of Ductile Materials 197: 23-32
12. Nelder, J.A., and R. Mead. 1965. A Simplex Method for Function Minimization. The Computer Journal. 4: 308-313
13. Ge, M. 2003 Analysis of source location algorithms part II: iterative methods[J]. Journal of Acoustic Emission 21(1), 29–51
14. Mistras Group. 2014. Express-8 AE System User's Manual.
15. Vorobiev, O.Y. 2012. Simple Common Plane contact algorithm. *Int. J. Num Meth in Engineering.* 90: 243–268.
16. Kobayashi, A., Ohtani, N., Sato, T. 1974. Phenomenological aspects of viscoelastic crack propagation. J. Appl. Poly. Sci., 18 , pp. 1625-1638
17. Vorobiev,O.Y., Robey, R.E., Pope, J., Torres, S.M., Hargather, M.J., 2022. Analysis and Modeling of Explosive Fracturing Process in a Transparent Surrogate of Jointed Rock. 56th US Rock Mechanics/Geomechanics Symposium. ARMA 22-90.